

Application of the Localised Lagrange Multiplier Method to a 3D Contact Patch Test

G. Rebel, K. C. Park, C. A. Felippa
Center for Aerospace Structures and
Department of Aerospace Engineering Sciences
University of Colorado at Boulder, Campus Box 429
Boulder, Colorado 80309-0429

10 August 2001

Abstract

The ability to represent constant stress states is an important issue in finite element analysis. State of the art elements are able to perform flawlessly for such states as long as meshes are conforming. When two domains share a boundary, their meshes do not match at the common boundary when no special care is taken. Sometimes it can be even impossible to make such meshes conforming like for instance in contact analysis with sliding. Patch tests for testing the transfer of constant stress states at nonconforming shared boundaries have been formulated for the 2D case. Here we intent to introduce such a test for the 3D case and demonstrate that the localised Lagrange multiplier approach can be used successfully to pass the 3D Patch test for nonconforming grids.

1 Introduction

The exact transfer of constant stress states is an important issue in finite element analysis. Finite elements should be designed such that they can pass so called constant stress patch tests. Application of elements that pass such tests in successively refined meshes is expected to converge to the correct analysis result when the mesh is conforming ^[8]. The meshes of two domains that have a common boundary are in general nonconforming when no special attention is given to the meshing at their shared boundary. In the case of contact analysis it can be even

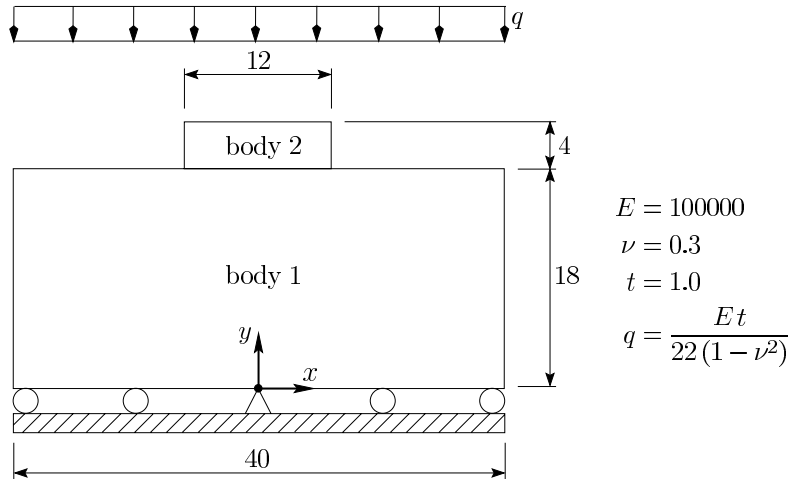


Figure 1: Plain strain 2D contact patch test problem.

impossible to generate conforming meshes especially when sliding occurs. The question then arises how well constant stress states are transmitted at the shared (nonconforming) boundary. To address this problem the 2D patch test for contact problems shown in Figure 1 has been proposed by Taylor and Papadopoulos ^[9,13]. The test consists of a flexible punch that comes into contact with a deformable foundation. Uniform loading q is applied to the free upper surface of both the punch and the foundation. Both bodies have the same elastic constants and the boundary conditions allow for free lateral expansion. An essential feature of this test is that the mesh at the shared boundary is nonconforming as shown in Figure 2.

In our approach for modelling contact problems, or more generally, modelling the connection between nonmatching grids, we place a frame endowed with its own nodal

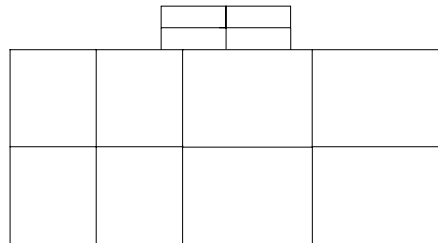


Figure 2: Nonconforming meshes at the shared boundary are an essential feature of the 2D contact patch test problem.

freedoms in between the nonconforming grids and then proceed to establish the connection between each side and the frame by means of *localised* Lagrange multipliers. By utilising the design freedom in the frame setup we demonstrated that the localised Lagrange multiplier method leads to perfect results in the 2D contact patch test problem ^[10,11].

The next step in the development of our frame based approach is its application to 3D problems. To this end we first designed a 3D contact patch test problem with similar features as its 2D counterpart. Then we applied the frame based approach to this problem. This paper will first introduce the proposed 3D contact patch test problem. For comparison purposes we briefly revisit the classical discrete formulation of contact problems in its Lagrange multiplier form. We then introduce the basic formulation of the frame based approach. Next, we discuss the discretisation of the frame and highlight the difference between the discrete frame based formulation and the classical approach. Finally, we present the results of the frame based approach for the proposed 3D contact patch test problem.

2 Proposed 3D contact patch test problem

The proposed 3D contact patch test problem is depicted in Figure 3. It has been designed such that it has similar features as its 2D counterpart. Once again, a flexible punch comes into contact with a deformable foundation. In general contact problems are expected to have contact domains with curved boundaries. This motivates our choice for a cylindrically shaped punch. Uniform pressure loading p is applied to the free upper surface of both the punch and the foundation. Both the foundation (body 1) and the punch (body 2) have the same elastic constants and the boundary conditions allow for free lateral expansion. Please notice that the rigid body rotation about the z -axis is suppressed at node A. The boundary conditions, material data and problem dimensions are given in Figure 3.

The proposed 3D contact patch test ideally produces a uniform stress field $\sigma_{zz} = -260$ and all other stresses are equal to zero. The Von Mises stress for this state is $\sigma_{\text{vonMises}} = 260$. The only nonzero strain components become

$$\varepsilon_{xx} = \varepsilon_{yy} = 0.03 \quad \text{and} \quad \varepsilon_{zz} = -0.1 \quad (1)$$

The entire top surface of the foundation should displace 0.1 downward, so that it still is a flat surface after deformation.

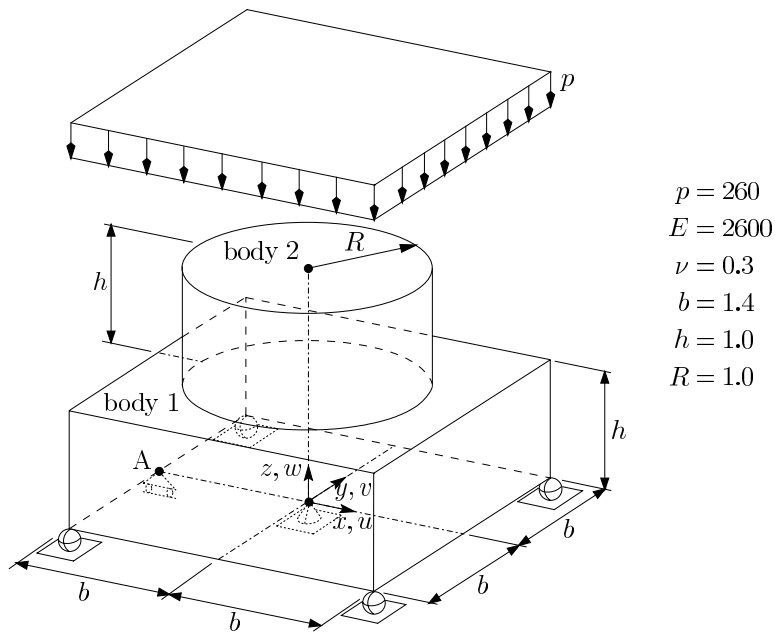


Figure 3: 3D contact patch test problem.

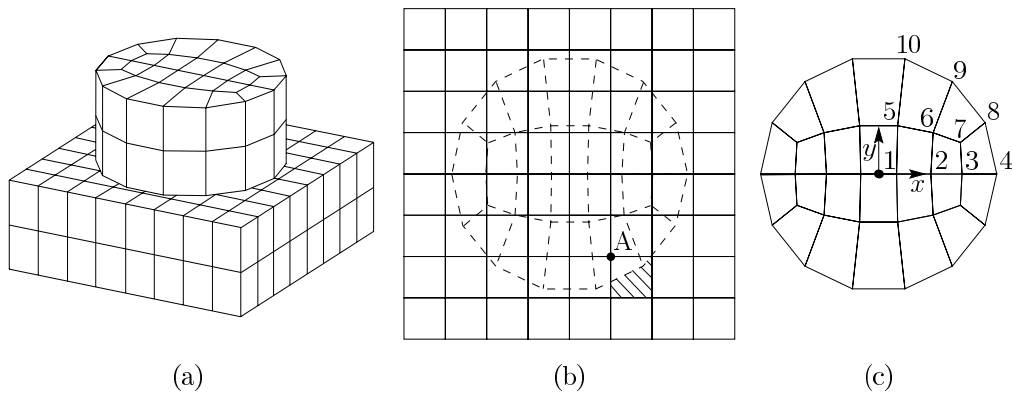


Figure 4: Discretisation of the 3D contact patch test model: (a) Finite element mesh. (b) Regular cross section mesh of the foundation. (c) Cross section mesh of the punch.

node	x	y
1	0.15104895	0.00000000
2	0.44055944	0.00000000
3	0.70629371	0.00000000
4	1.00000000	0.00000000
5	0.16083916	0.40839161
6	0.46153846	0.34965035
7	0.69230769	0.26573427
8	0.90096887	0.43388374
9	0.62348980	0.78183148
10	0.22252093	0.97492791

Table 1: Initial cross section nodal coordinates of the punch (see Figure 4_c for the node numbering).

An essential feature of a contact patch test problem is the use of nonmatching meshes at the contact surface. Figure 4 shows the discretisation we have used in the analysis. The meshes of the punch and foundation are clearly nonmatching. The foundation has a regular mesh in all three dimensions. The meshing of the punch is shown in Figure 4_c, whereas the corresponding nodal coordinates are listed in Table 1. Please notice that the cross section meshes are chosen symmetric about the x and y axes.

The uniform pressure loading needs to be translated in energy equivalent nodal forces. This pressure is applied to the free top surfaces of both the punch and foundation. As a result some element faces of the top surface of the foundation will be loaded only partially like this is indicated by the shaded area in Figure 4_b. Such a partially loaded element face will produce energy equivalent forces at nodes that are inside the contact domain (for example node A in Figure 4_b). Numerical integration has been employed to obtain the energy equivalent forces to be placed on the model. Since it is the objective of the test to find zero error from the theoretical solution it is of the utmost importance to obtain these forces accurately. In our case, energy equivalent forces have been computed up to at least 8 decimal places accuracy.

3 Classical discrete approach

The discrete approach in the treatment of contact impact problems is attractive since it avoids integration problems related to the use of surface tractions in the

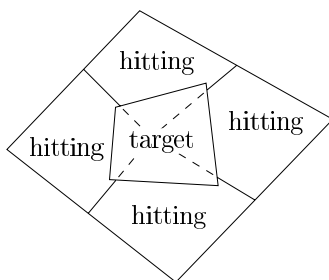


Figure 5: A target segment in contact with several hitting segments.

modelling of the interaction between contacting bodies. To illustrate this consider the computation of the virtual work due to these tractions, which is defined as

$$\delta W_{\text{contact}} = \iint_{\mathcal{A}_c^{(h)}} \mathbf{t}^{(h)} \cdot \delta \mathbf{u}^{(h)} d\mathcal{A} + \iint_{\mathcal{A}_c^{(t)}} \mathbf{t}^{(t)} \cdot \delta \mathbf{u}^{(t)} d\mathcal{A} = \iint_{\mathcal{A}_c^{(t)}} \mathbf{t}^{(t)} \cdot (\delta \mathbf{u}^{(t)} - \delta \mathbf{u}^{(h)}) d\mathcal{A}$$

The two sides are indicated by superindex (t) for "target" and superindex (h) for "hitting". This virtual work can be computed by choosing one of the contacting sides as target surface and then integrate over this target surface ^[16] (the other contact side is then referred to as hitting surface). The discrete target and hitting surfaces can be thought of as a collection of surface segments in the finite element model. The integration over the target surface thus becomes a summation of integrations over target segments. All variables in the virtual work integrand are interpolated using the discretisation of the target surface except for the displacement of the hitting surface $\mathbf{u}^{(h)}$. A problem now arises in dealing with the displacement of the hitting surface. This is because several hitting segments can come in contact with one target segment (see Figure 5). Although it is theoretically possible to express the hitting surface displacement by using several different functions and carry out the target segment integration as a summation of several surface integrations, it is practically inconvenient to do so. A more practical approach can be found by viewing the tractions as ordinary external loads on each of the bodies or domains. In the context of the finite element method such tractions are applied to the model through energy equivalent forces at nodal points. Of course, the difference with ordinary external loads is that their magnitude is unknown a priori. To circumvent the integration difficulty many researchers ^[1,3-6,12,14,15] take these unknown nodal forces directly as primary unknowns instead of the unknown traction. This leads to the so-called discrete classical formulation of the contact problem. In the remaining part of this section we will give a specific example of such a discrete formulation

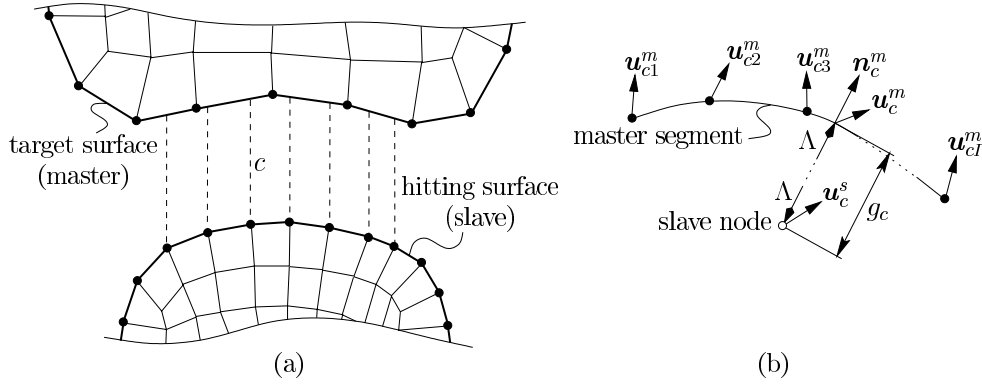


Figure 6: (a) Discrete contact between a hitting surface and a target surface in the master-slave approach. (b) Slave node in contact with a master segment. The master segment displacement is interpolated using I nodes.

which will serve to compare our frame based formulation with the classical formulation. To this end only the linear case needs to be considered.

The master-slave ^[16] approach depicted in Figure 6 is an example of a discrete contact formulation. One of the contacting sides is chosen as hitting (slave) surface and the other as target (master) surface. Only nodes on the hitting boundary are prohibited to penetrate the segments of the target boundary. Penetration of target nodes through hitting segments is ignored. A non-penetration constraint is constructed for each hitting node \sim target segment pair (contact pair). Considering only small displacements, the constraint for contact pair c can be written as

$$\mathbf{n}_c^m \cdot (\mathbf{u}_c^m - \mathbf{u}_c^s) + g_c = \mathbf{Q}_c \mathbf{u}_c + g_c = 0 \quad \text{with: } c = 1, \dots, C \quad (2)$$

where

$$\begin{aligned}
\mathbf{u}_c^m &= \text{displacement vector of the master surface at } c = \sum_{i=1}^I N_i \mathbf{u}_{ci}^m \\
\mathbf{u}_c^s &= \text{displacement vector of the slave node at } c \\
\mathbf{n}_c^m &= \text{normal to the master surface at } c \\
g_c &= \text{initial normal gap at } c \\
\mathbf{u}_{ci}^m &= \text{displacement vector of the master surface at master node } i \\
N_i &= \text{shape function associated with master node } i \\
\mathbf{Q}_c &= (\mathbf{n}_c^m)^t [-\mathbf{I} \ N_1 \mathbf{I} \ \cdots \ N_I \mathbf{I}]_c \\
(\mathbf{u}_c)^t &= [(\mathbf{u}_c^s)^t \ (\mathbf{u}_{c1}^m)^t \ \cdots \ (\mathbf{u}_{cI}^m)^t]
\end{aligned}$$

Assembling all non-penetration constraints in one equation we arrive at

$$\mathbf{Q} \mathbf{u} + \mathbf{g} = \mathbf{0} \quad (3)$$

The potential energy for a linear static mechanical problem is written in its unconstrained form as

$$\Pi(\mathbf{u}) = \frac{1}{2} \mathbf{u}^t \mathbf{K} \mathbf{u} - \mathbf{u}^t \mathbf{f} \quad (4)$$

where \mathbf{u} is the global displacement vector, \mathbf{K} the global stiffness matrix and \mathbf{f} the global load vector. Equation (4) represents the linear quasi static behaviour of all the bodies in contact without taking into account their contact interactions. In the Lagrange multiplier method, the non-penetration constraints are introduced by replacing $\Pi(\mathbf{u})$ by

$$\Pi_{\text{constrained}}(\mathbf{u}) = \frac{1}{2} \mathbf{u}^t \mathbf{K} \mathbf{u} - \mathbf{u}^t \mathbf{f} + \boldsymbol{\lambda}^t (\mathbf{Q} \mathbf{u} + \mathbf{g}) \quad (5)$$

The third term in this expression represents the potential $-\delta W_{\text{contact}}$ of the discrete contact forces. The constrained minimisation problem (5) has the solution

$$\begin{bmatrix} \mathbf{K} & \mathbf{Q}^t \\ \mathbf{Q} & \mathbf{0} \end{bmatrix} \begin{bmatrix} \mathbf{u} \\ \boldsymbol{\lambda} \end{bmatrix} = \begin{bmatrix} \mathbf{f} \\ -\mathbf{g} \end{bmatrix} \quad (6)$$

The Lagrange multipliers $\boldsymbol{\lambda}$ are interpreted as contacting forces at corresponding hitting node locations.

Remark 3.1 *The classical master-slave approach depends heavily on discretisation details of the master surface. Therefore, even though its discrete nature circumvents integration problems, it is still not generic. This dependence can be eliminated in our discrete frame based approach.*

Remark 3.2 *The displacement constraint operator \mathbf{Q} is a sparse matrix in the classical master-slave method. In section 6 we will recast our frame based formulation in the form (6) to reveal that a patch test passing constraint operator \mathbf{Q} is in general dense.*

4 Frame based contact model

The frame based contact model has been discussed in detail in ^[10]. In this paper we intend to look at a specific detail of the formulation, namely, how to design a 3D contact frame that has the ability to pass the contact patch test. To reach this objective we first need to identify which part of the formulation is responsible for this behaviour. In this section we will revisit the frame based contact model and identify the equation that governs the contact patch test passing behaviour. In section 6 we will cast the discrete frame based formulation in the form (6) for comparison with the classical discrete approach. This leads to a general statement regarding patch test passing behaviour of the latter.

Figure 7 shows the expanded view of two bodies in contact. A contact frame is placed at the original contact position. The vertical dashed lines indicate corresponding points on the bodies and the contact frame. That is, the points connected by the vertical dashed lines have identical positions in space.

The contact frame is introduced as a new element in the description of contact-impact problems. Each body contacts one of its sides and exerts forces on the frame. The total force system on the contact frame is then required to be in self

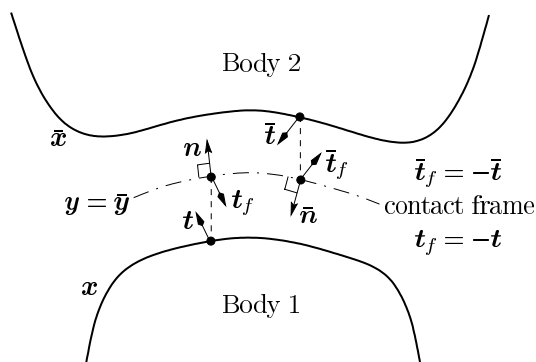


Figure 7: Expanded view of contact between two bodies with a contact frame placed in between

equilibrium. The contact frame can be seen as a transducer that transfers the action of one body onto the other in a way that satisfies momentum balance.

The motion of body 1 is described by a displacement \mathbf{u} from its reference position \mathbf{X} . The motion of body 2 is described by a displacement $\bar{\mathbf{u}}$ from its reference position $\bar{\mathbf{X}}$. The current positions \mathbf{x} and $\bar{\mathbf{x}}$ of bodies 1 and 2 respectively, are thus given by

$$\mathbf{x} = \mathbf{X} + \mathbf{u} \quad ; \quad \bar{\mathbf{x}} = \bar{\mathbf{X}} + \bar{\mathbf{u}} \quad (7)$$

and are indicated in Figure 7.

The description of the motion of the contact frame should include the rigid body motions. Moreover, it should be able to deform so that the bodies on either side can deform during contact. The position \mathbf{y} of the contact frame is composed of a reference position \mathbf{Y} and a relative displacement \mathbf{v} such that

$$\mathbf{y} = \mathbf{Y} + \mathbf{v} \quad (8)$$

We choose the reference position \mathbf{Y} to be the *current* position of the contact frame. We also introduce the notation $\bar{\mathbf{y}}$ for the position of the contact frame. By definition we set $\bar{\mathbf{y}}$ equal to \mathbf{y} and we have

$$\bar{\mathbf{y}} = \bar{\mathbf{Y}} + \bar{\mathbf{v}} \quad \text{with: } \bar{\mathbf{Y}} = \mathbf{Y} \text{ and } \bar{\mathbf{v}} = \mathbf{v} \quad (9)$$

Let \mathbf{y} describe the contact frame side where body 1 contacts and let $\bar{\mathbf{y}}$ correspond to the contact frame side where body 2 contacts. This makes it possible to use similar notations for the description of the contact on either side of the contact frame. Also it allows different descriptions of the *same* contact frame depending on the side of contact.

The components of the contact traction \mathbf{t}_f in the normal and tangential directions of the contact surface play an important role in contact-impact analysis. We use a locally orthonormal base system \mathbf{a}_i (with $i = \{1, 2, 3\}$) at each contact frame point to describe this decomposition of \mathbf{t}_f . We choose $\mathbf{n} = \mathbf{a}_3$ to be the normal to the contact frame. On the opposing side of the contact frame we define $\bar{\mathbf{a}}_i = -\mathbf{a}_i$. Using these definitions, the decomposition of the contact tractions become

$$\mathbf{t}_f = -\mathbf{t} = \lambda^i \mathbf{a}_i \quad ; \quad \bar{\mathbf{t}}_f = -\bar{\mathbf{t}} = \bar{\lambda}^i \bar{\mathbf{a}}_i \quad (10)$$

Throughout this paper summation will be implied by indices that appear both as upper and as lower indices in one term. The special notation $\lambda = \lambda^3$ is introduced for the normal component of the contact traction. Finally, we choose the orientation of the normal \mathbf{n} such that λ is positive in compression as illustrated in Figure 7. The choice for base system $\bar{\mathbf{a}}_i$ is motivated by the fact that it sets $\lambda^i = \bar{\lambda}^i$ in the continuum description as a result of momentum balance.

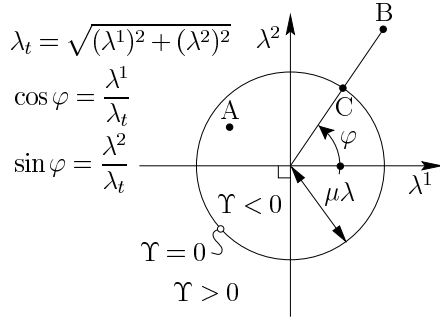


Figure 8: Friction yield function.

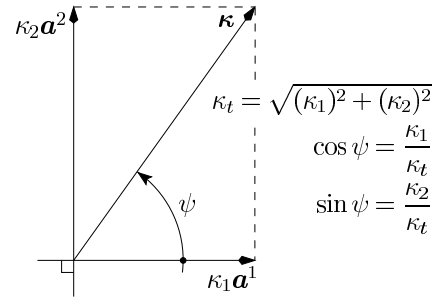


Figure 9: Direction of slip displacement.

In the case of frictional contact, the local conditions on the contact surface prescribe whether a state of stick (resp. slip), where the relative velocity is zero (resp. non-zero), will persist. Basically, we follow the approach advocated in [7] to implement these two states. A constitutive framework is needed to discern the two states and transitions between them. To this end, define a single yield function

$$\Upsilon = \sqrt{(\lambda^1)^2 + (\lambda^2)^2} - \mu \lambda \quad (11)$$

in which μ represents the Coulomb friction coefficient. On the opposing side of the contact frame a similar yield function $\bar{\Upsilon}$ is defined. However, since the surface characteristics are the same on both sides of the contact frame we have $\mu = \bar{\mu}$. The yield function is required to be negative or zero. A negative value $\Upsilon < 0$ represents a state of stick while slip will be incipient for $\Upsilon = 0$. Hence, the traction $\lambda^\alpha \mathbf{a}_\alpha$ (with $\alpha = \{1, 2\}$) has to remain inside ($\Upsilon < 0$) or on ($\Upsilon = 0$) a circular yield surface $\Upsilon = 0$ with radius $\mu \lambda$ (see Figure 8).

The gap normal to the contact surface has to remain zero on the contact surface. Mathematically this can be written as

$$\begin{aligned} \mathbf{x} - \mathbf{y} &= \boldsymbol{\kappa} & \text{with: } \boldsymbol{\kappa} &= \kappa^\alpha \mathbf{a}_\alpha = \kappa_\alpha \mathbf{a}^\alpha \quad (\mathbf{a}_\alpha = \mathbf{a}^\alpha \text{ and } \kappa_\alpha = \kappa^\alpha) \\ \bar{\mathbf{x}} - \bar{\mathbf{y}} &= \bar{\boldsymbol{\kappa}} & \text{with: } \bar{\boldsymbol{\kappa}} &= \bar{\kappa}^\alpha \bar{\mathbf{a}}_\alpha = \bar{\kappa}_\alpha \bar{\mathbf{a}}^\alpha \quad (\bar{\mathbf{a}}_\alpha = \bar{\mathbf{a}}^\alpha \text{ and } \bar{\kappa}_\alpha = \bar{\kappa}^\alpha) \end{aligned} \quad (12)$$

This equation allows slip displacements $\boldsymbol{\kappa}$ and $\bar{\boldsymbol{\kappa}}$ tangent to the contact frame. These slip displacements cannot be independent since that would leave the tangential motion of the contact frame undefined. To deal with this we set

$$\kappa_\alpha = \bar{\kappa}_\alpha \quad (13)$$

which defines the tangential motion of the frame to be the *average* of the tangential motion of the two bodies on either side of the contact surface. The gap constraints (12) are decomposed in normal and tangential directions and enforced in a weak sense using the variational form

$$\begin{aligned} \pi_c^{\text{total}} = & \iint_{\mathcal{A}_c} (\delta\{\lambda \mathbf{n} \cdot (\mathbf{x} - \mathbf{y})\} + \delta\{\lambda^\alpha \mathbf{a}_\alpha \cdot (\mathbf{x} - \mathbf{y})\} + \\ & + \delta\{\gamma \kappa_\alpha (\lambda_l^\alpha - \lambda^\alpha) + \frac{1}{2} (1 - \gamma) \kappa_\alpha \kappa^\alpha\}) d\mathcal{A} + \\ & + \iint_{\bar{\mathcal{A}}_c} (\delta\{\bar{\lambda} \bar{\mathbf{n}} \cdot (\bar{\mathbf{x}} - \bar{\mathbf{y}})\} + \delta\{\bar{\lambda}^\alpha \bar{\mathbf{a}}_\alpha \cdot (\bar{\mathbf{x}} - \bar{\mathbf{y}})\} + \\ & + \delta\{\bar{\gamma} \bar{\kappa}_\alpha (\bar{\lambda}_l^\alpha - \bar{\lambda}^\alpha) + \frac{1}{2} (1 - \bar{\gamma}) \bar{\kappa}_\alpha \bar{\kappa}^\alpha\}) d\bar{\mathcal{A}} \end{aligned} \quad (14)$$

To discuss this variational form let us investigate the integrand over \mathcal{A}_c , i.e., the contact between body 1 and the frame. We introduced the Lagrange multipliers λ , λ^α to enforce the gap constraint $\mathbf{x} - \mathbf{y} = \boldsymbol{\kappa}$ in normal and tangential directions. These Lagrange multipliers are the components of the contact tractions in equation (10). The contact domain \mathcal{A}_c is defined by the conditions

$$\mathbf{n} \cdot (\mathbf{x} - \mathbf{y}) = 0 \quad \text{where} \quad \lambda \geq 0 \quad (15)$$

The third and fourth terms of the integrand govern the sliding behaviour of the model. Parameter γ is used as switch to either allow a point \mathbf{x} to slide along the frame ($\gamma = 1$) or prohibit this sliding ($\gamma = 0$). This parameter is a function of position.

Two issues remain to be discussed, namely, when to switch between stick and slip states and how to define the constraint on the frictional force in the slip state. These issues are interconnected and resolved as follows. At the start of an analysis we have no knowledge about the appropriate state and assume the whole system is in a sticking state and set $\gamma = 0$ everywhere. This forces the slip displacement $\boldsymbol{\kappa}$ to be zero. Suppose that the resulting deformed configuration does not violate the yield condition, i.e., $\Upsilon \leq 0$ everywhere, so that no further action needs to be taken. Let all frictional tractions for this configuration be inside the yield surface (illustrated by point A in Figure 8). Increased loading will at some instant reach the transition state where $\Upsilon = 0$ and $\boldsymbol{\kappa} = 0$. This state still satisfies balance of linear momentum and the stick state is taken to persist. Further loading finally violates the yield condition $\Upsilon \leq 0$ (illustrated by point B in Figure 8) and we need to switch to the slip state and have to set $\gamma = 1$ at such points. The direction of the frictional forces is defined by $\Upsilon = 0$ as being opposite to the direction of sliding. However, if the previous state was a sticking state, we have no previous sliding direction available and simply map the frictional force back to the yield surface in radial direction using (see point C in Figure 8)

$$\lambda_l^1 = \mu \lambda \cos \varphi \quad ; \quad \lambda_l^2 = \mu \lambda \sin \varphi \quad (16)$$

in which angle φ defines the direction of the frictional force in the previous iterate. When the previous state is a slipping state, a nonzero slipping direction is available. Therefore, we can set the constitutive equation that defines the frictional forces such that it is consistent with the yield condition $\Upsilon = 0$ and use (see Figure 9)

$$\lambda_l^1 = -\mu \lambda \cos \psi \quad ; \quad \lambda_l^2 = -\mu \lambda \sin \psi \quad (17)$$

in which angle ψ defines the direction of slip in the previous iterate. The convergence to the balance of linear momentum provides a direction of slip until the point of transition $\Upsilon = 0$ and $\boldsymbol{\kappa} = 0$ is reached again. Directional dependence of the frictional forces then becomes unavailable and we switch back to the stick state $\gamma = 0$. It is noted that the limiting values λ_l^α are set based on the previous iterate. We note also that the conditions used here to deal with the stick/slip states correspond precisely to those developed in reference [2] for rigid plasticity. For the frictionless case, we can use $\mu = 0$ in our model and the difference between the constitutive definitions (16) and (17) vanishes.

After rewriting the expression for $\delta\pi_c^{\text{total}}$ in terms of the variational fields, we obtain as first variation for the complete contact system [10]

$$\delta\pi = \delta\pi_{\text{free}}^{\text{total}} + \delta\pi_c^{\text{total}} \quad (18)$$

where

$$\begin{aligned} \pi_{\text{free}}^{\text{total}} = \delta\pi_{\text{free}} + \delta\bar{\pi}_{\text{free}} & \quad ; \quad \delta\pi_c^{\text{total}} = \delta\pi_c + \delta\bar{\pi}_c \\ \delta\pi_{\text{free}} = G & \quad ; \quad \delta\pi_c = G_{c\lambda} - G_{cu} + G_{c\kappa} - G_{cv} \\ \delta\bar{\pi}_{\text{free}} = \bar{G} & \quad ; \quad \delta\bar{\pi}_c = \bar{G}_{c\lambda} - \bar{G}_{cu} + \bar{G}_{c\kappa} - \bar{G}_{cv} \end{aligned}$$

in which $G(\mathbf{x}; \delta\mathbf{u})$ and $\bar{G}(\bar{\mathbf{x}}; \delta\bar{\mathbf{u}})$ are the first variations of the two bodies excluding contact, and the remaining expressions are given by

$$\begin{aligned} G_{c\lambda}(\mathbf{x}, \mathbf{y}, \kappa_\alpha; \delta\lambda, \delta\lambda^\alpha) &= \iint_{\mathcal{A}_c} (\delta\lambda \{ \mathbf{n} \cdot (\mathbf{x} - \mathbf{y}) \} + \delta\lambda^\alpha \{ \mathbf{a}_\alpha \cdot (\mathbf{x} - \mathbf{y}) - \gamma \kappa_\alpha \}) d\mathcal{A} \\ G_{cu}(\mathbf{y}, \lambda, \lambda^\alpha; \delta\mathbf{u}) &= \iint_{\mathcal{A}_c} (-\delta\mathbf{u} \cdot \{ \lambda \mathbf{n} + \lambda^\alpha \mathbf{a}_\alpha \}) d\mathcal{A} \\ G_{c\kappa}(\mathbf{y}, \lambda^\alpha, \kappa^\alpha; \delta\kappa_\alpha) &= \iint_{\mathcal{A}_c} (\delta\kappa_\alpha \{ \gamma (\lambda_l^\alpha - \lambda^\alpha) + (1 - \gamma) \kappa^\alpha \}) d\mathcal{A} \\ G_{cv}(\mathbf{x}, \mathbf{y}, \lambda, \lambda^\alpha; \delta\mathbf{v}) &= \iint_{\mathcal{A}_c} (\delta\mathbf{v} \cdot \{ \lambda \mathbf{n} + \lambda^\alpha \mathbf{a}_\alpha \} - \delta\mathbf{v}_{,\alpha} \cdot \{ \mathbf{Q}_\alpha \Phi^\alpha(\mathbf{x} - \mathbf{y}) \}) d\mathcal{A} \end{aligned} \quad (19)$$

where

$$(\cdot)_{,\alpha} = \frac{\partial(\cdot)}{\partial \xi^\alpha}, \mathbf{a}_\alpha = \frac{1}{\|\mathbf{y}_{,\alpha}\|} \mathbf{y}_{,\alpha}, \mathbf{Q}_\alpha = \frac{1}{\|\mathbf{y}_{,\alpha}\|} (\mathbf{I} - \mathbf{a}_\alpha \otimes \mathbf{a}_\alpha), \mathbf{\Phi}^\alpha = \lambda^\alpha \mathbf{I} + \lambda e^{\alpha\beta} (\mathbf{a}_\beta \times \mathbf{I})$$

It should be noted that $G_{c\lambda}(\mathbf{x}, \mathbf{y}, \kappa_\alpha; \delta\lambda, \delta\lambda^\alpha)$ constitutes the kinematic constraint between the contact surface \mathbf{x} and contact frame \mathbf{y} , $G_{cu}(\mathbf{y}, \lambda, \lambda^\alpha; \delta\mathbf{u})$ the virtual work of the contact traction acting on contact surface \mathbf{x} , $G_{c\kappa}(\mathbf{y}, \lambda^\alpha, \kappa^\alpha; \delta\kappa_\alpha)$ the constraint on the frictional behaviour, and $G_{cv}(\mathbf{x}, \mathbf{y}, \lambda, \lambda^\alpha; \delta\mathbf{v})$ the virtual work of the contact traction acting on contact frame \mathbf{y} , respectively. Similarly, the four corresponding terms in $\delta\bar{\pi}_c$ can also be identified.

Setting the first variation $\delta\pi$ equal to zero yields among others the equilibrium equation of the contact frame

$$G_{cv}(\mathbf{x}, \mathbf{y}, \lambda, \lambda^\alpha; \delta\mathbf{v}) + \bar{G}_{cv}(\bar{\mathbf{x}}, \bar{\mathbf{y}}, \bar{\lambda}, \bar{\lambda}^\alpha; \delta\bar{\mathbf{v}}) = 0 \quad (20)$$

This equation accounts for equilibrium in the contact domain. Specifically, this equation results since the contact frame surface is endowed with independent kinematic variables \mathbf{v} (or $\bar{\mathbf{v}}$). It is the only equation that is *nonlocal*. All other equations are strictly local to one side of the contact frame. It acts as a force transducer between the two sides. Discretisation of this transducer will limit its set of solutions. Therefore a discrete version of the transducer should be designed such that the intended solution is contained in its solution set. In order to pass a contact patch test we should guide the design of the frame by the requirement that the correct patch test solution is among the possible discrete solutions. This will be the topic of the next section.

5 Design of a flat contact frame

The design of the contact frame will be based on the condition that it should be able to transfer a constant normal pressure field exactly. In this section we will consider a flat contact domain as shown in Figure 10_a. It shows two bodies in contact with a constant normal pressure field in between. This contact system is replaced by its discrete version in Figure 10_b. The constant pressure field has been replaced by energy equivalent forces acting at nodal points of each of the bodies. These forces are applied as lumped forces to each side of the contact surface. This can produce energy equivalent forces to be applied outside the original contact domain since some faces of the body elements are only partially loaded. To capture these forces, the discrete contact domain (contact frame) can be an expanded version of the original contact

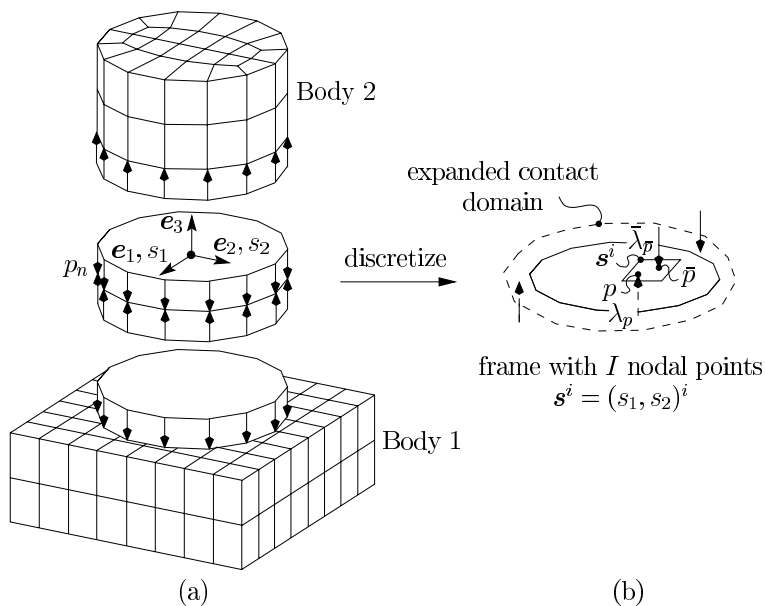


Figure 10: (a) Constant normal pressure in the contact domain. (b) Discrete energy equivalent forces (corresponding to the constant normal pressure field) acting as lumped forces on the contact frame.

domain. This is indicated by the dashed line in Figure 10_b, which surrounds the original contact domain indicated by the solid line. For future reference it is convenient to define a contact pair at this point. This is the combination of a nodal point of one of the contacting bodies and the point on the frame it touches.

The constant normal pressure fields on both contacting sides are represented by a set of energy equivalent forces. These forces form the set of patch test passing forces. They are substituted in equation (20) in order to obtain the equation used in the design process of the frame. Mathematically this substitution involves expressing the normal pressure fields λ and $\bar{\lambda}$ in terms of the set of patch test passing forces utilising Dirac delta functions. After choosing a frame discretisation and carrying out the integrations we arrive at the discrete frame equilibrium equation. In general, this equation will be violated for an arbitrary frame discretisation. However, we still have the nodal positions of our frame as unknowns in the model. Therefore, we can attempt to move these nodes into positions such that our weak form of momentum balance is no longer violated for the given set of collocated patch test passing forces. The resulting frame will be a contact patch test passing frame by design and is appropriate for use in numerical simulations. In the remaining part of this section we will first derive the condition that has to be satisfied in the design process and then

apply the design procedure to our proposed 3D contact patch test.

To obtain the equations to be used in the frame design process, we first note that the intended solution has the properties

$$\lambda \mathbf{n} + \lambda^\alpha \mathbf{a}_\alpha = p_n \mathbf{e}_3 \quad ; \quad \mathbf{x} - \mathbf{y} = \mathbf{0} \quad (21)$$

throughout the contact domain \mathcal{A}_c . Inserting this into the expression for G_{cv} yields (with $\mathbf{v} = v^1 \mathbf{e}_1 + v^2 \mathbf{e}_2 + v \mathbf{e}_3$)

$$G_{cv} = \iint_{\mathcal{A}_c} \delta \mathbf{v} \cdot p_n \mathbf{e}_3 d\mathcal{A} = \iint_{\mathcal{A}_c} \delta v p_n d\mathcal{A} \quad (22)$$

This equation needs to be obtained in discrete form which requires the specification of the frame displacement and pressure discretisation.

The frame is discretised by standard isoparametric 4-noded bilinear elements so that we have

$$v^e = \sum_{J=1}^4 N_J v_J^e = [N_1 \ N_2 \ N_3 \ N_4] \begin{bmatrix} v_1^e \\ v_2^e \\ v_3^e \\ v_4^e \end{bmatrix} \quad (23)$$

with $(\xi \in [-1, +1]$ and $\eta \in [-1, +1])$

$$\begin{aligned} N_1 &= \frac{1}{4} (1 - \xi)(1 - \eta) \quad ; \quad N_2 = \frac{1}{4} (1 + \xi)(1 - \eta) \\ N_3 &= \frac{1}{4} (1 + \xi)(1 + \eta) \quad ; \quad N_4 = \frac{1}{4} (1 - \xi)(1 + \eta) \end{aligned}$$

within frame element e . The coordinates ξ and η are the usual parametric coordinates.

The constant normal pressure field has been converted to energy equivalent nodal forces applied at nodal points of the contacting bodies. To represent these lumped forces we use the Dirac delta function δ . Using the notation $\mathbf{s} = (s_1, s_2) \in \mathcal{A}_c$ for the surface coordinates of the contact domain, we define this delta function as

$$\iint_{\mathcal{A}_c} f(\mathbf{s}) \delta(\mathbf{s} - \mathbf{s}_p) d\mathcal{A} = f(\mathbf{s}_p) \quad (24)$$

where $\delta \rightarrow \infty$ for $\mathbf{s} \rightarrow \mathbf{s}_p$ and δ equal to zero outside an infinitesimal region around $\mathbf{s} = \mathbf{s}_p$. The pressure field corresponding to a lumped energy equivalent force λ_p applied at point p can now be given as

$$p_n(\mathbf{s}) = \lambda_p \delta(\mathbf{s} - \mathbf{s}_p) \quad (25)$$

To obtain the discrete form of equation (22), we first convert the integrations over the contact domain to summations over contact pairs. Hence we write

$$\iint_{\mathcal{A}_c} (\dots) d\mathcal{A} = \sum_{p=1}^P \iint_{\mathcal{A}_p} (\dots) d\mathcal{A} \quad ; \quad \iint_{\bar{\mathcal{A}}_c} (\dots) d\bar{\mathcal{A}} = \sum_{\bar{p}=1}^{\bar{P}} \iint_{\bar{\mathcal{A}}_{\bar{p}}} (\dots) d\bar{\mathcal{A}}$$

in which capital P and \bar{P} represent the total number of contact pairs on either side of the contact frame. Also, we need to define a finite element assembly operator in order to extract the normal frame displacement local to a specific contact pair from the global vector of normal frame displacements \mathbf{v} . Therefore, introduce

$$\begin{bmatrix} v_1^e \\ v_2^e \\ v_3^e \\ v_4^e \end{bmatrix}_p = \mathcal{L}_{vp} \mathbf{v} \quad ; \quad \mathbf{v}^t = [v_1 \cdots v_I] \quad (26)$$

Substituting the discretisation in expression (22) for G_{cv} and carrying out the integrations, we arrive at the expression

$$G_{cv} = \delta \mathbf{v} \cdot \mathbf{p} \quad ; \quad \mathbf{p} = \sum_{p=1}^P \mathcal{L}_{vp}^t \mathbf{p}_p \quad ; \quad \mathbf{p}_p = \lambda_p \begin{bmatrix} N_1 \\ N_2 \\ N_3 \\ N_4 \end{bmatrix} \quad (27)$$

A similar expression can be found for \bar{G}_{cv} . The discrete version of the weak form of frame equilibrium (20) is found to be

$$\delta \mathbf{v} \cdot (\mathbf{p} + \bar{\mathbf{p}}) = 0 \quad \text{with: } \mathbf{p}^t = [p_1 \cdots p_I] \quad \text{and} \quad \bar{\mathbf{p}}^t = [\bar{p}_1 \cdots \bar{p}_I] \quad (28)$$

This equation simply states that the assembled normal force has to be zero at each frame nodal point. We can satisfy this equation for the given patch test passing force system by finding appropriate nodal positions for the frame nodes. Essentially this frame design process is an optimisation problem. To cast this problem in the conventional optimisation form we formulate an objective function f in the form

$$f(\mathbf{s}) = \sum_{i=1}^I (p_i + \bar{p}_i)^2 \quad ; \quad \mathbf{s}^t = [(\mathbf{s}^1)^t \cdots (\mathbf{s}^I)^t] \quad (29)$$

and solve for $f(\mathbf{s}) = 0$ to find the optimum contact frame design. It is noted at this point that the magnitude as well as the point of application of the forces are given in equation (28). However, the parametric coordinates (ξ, η) of the frame element they

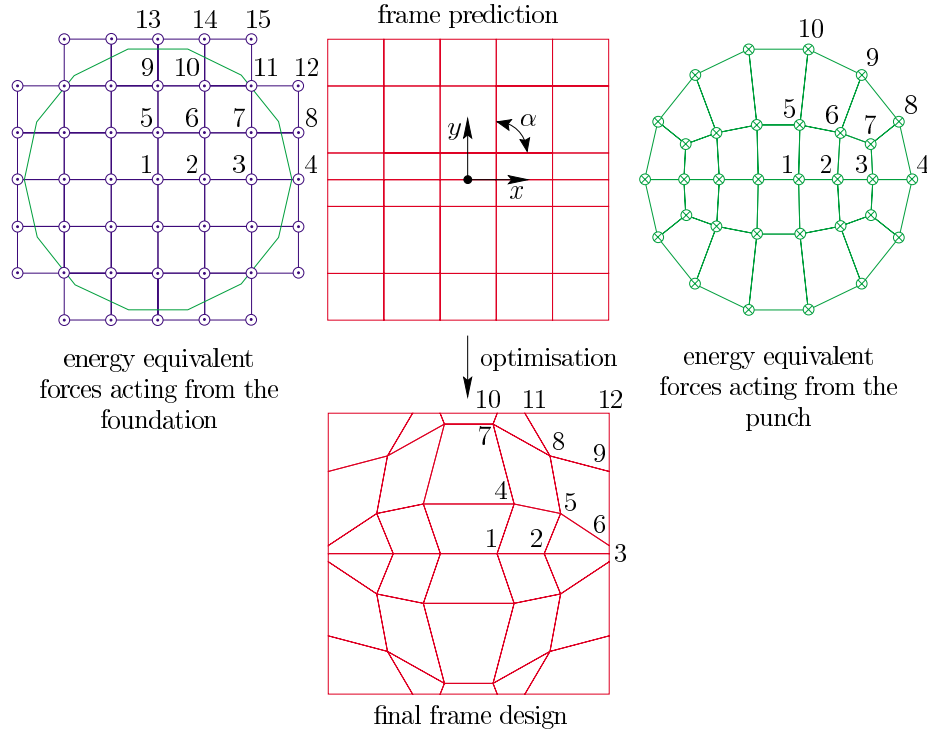


Figure 11: Frame design for the 3D contact patch test.

touch and even the touched frame element can change during the optimisation run. Finally, the optimisation will result in a frame design that has the patch test passing force set in its solution space. This gives our formulation its patch test passing quality.

The frame design procedure is now applied to the proposed 3D contact patch test problem. The design procedure is illustrated in Figure 11. The first step is to apply the constant pressure field to both the foundation and the punch in the contact domain. The punch will be loaded in its entire cross section which yields energy equivalent forces as indicated on the right in Figure 11. The foundation will be loaded by normal pressure inside the indicated green border and this yields energy equivalent forces as indicated on the left of the figure. A prediction for the frame is then created to which the set of patch test passing energy equivalent forces are applied. We have chosen a structured frame mesh of 42 nodes which is in between the number of body nodes in the contact domain on either side of the frame (32 for the punch and 45 for the foundation). Next, we solved the optimisation problem for the patch test passing frame design. We have used equality as well as inequality

node	prediction		final (optimised)	
	x	y	x	y
1	0.21	0.00	0.21146205	0.00000000
2	0.63	0.00	0.56401530	0.00000000
3	1.05	0.00	1.05000000	0.00000000
4	0.21	0.20	0.33965412	0.37074965
5	0.63	0.20	0.68689175	0.30017002
6	1.05	0.20	1.05000000	0.06001071
7	0.21	0.70	0.18146139	0.96891706
8	0.63	0.70	0.60713299	0.73075863
9	1.05	0.70	1.05000000	0.61430709
10	0.21	1.05	0.21312353	1.05000000
11	0.63	1.05	0.41996074	1.05000000
12	1.05	1.05	1.05000000	1.05000000

Table 2: Initial and final (optimised) frame nodal positions for the 3D contact patch test (see Figure 11 for the frame node numbering).

constraints to guide the optimisation process. Firstly, equality constraints are used to maintain the double symmetry in the frame design. Further, frame corner nodes are kept in place and nodes on the boundary of the contact domain are required to stay on straight lines in between the frame corner nodes. Inequality constraints are used to enforce that the corner node angle α at each corner of a frame element be in between 25° and 155° . Also, we required that the length of element sides be at least 0.06. These inequality constraints ensure that the element shape remains admissible. The resulting (optimised) frame is shown in the lower half of Figure 11 and the corresponding frame node positions are given in Table 2. The value of the objective function (29) is $\mathcal{O}(10^{-13})$ for this frame design. The way the foundation and punch are in contact with the optimised frame is illustrated in Figure 12.

6 Localised and classical formulations compared

In this section we compare our frame based formulation with the classical formulation. We will show that the contact enforcement operator \mathbf{Q} (see equation (6)) of the classical formulation needs to be a dense matrix in order for this formulation to pass the contact patch test. For this purpose we need the discrete form of variational equation (14) in its linearised form about the reference

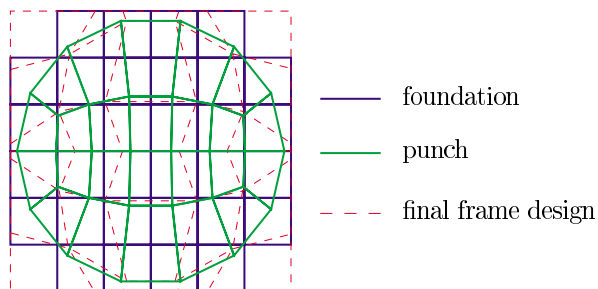


Figure 12: Discrete contact domains of the punch and foundation in contact with the optimised frame.

configuration. We then recast the governing equations of the discrete frame based contact model into the classical form (6) by eliminating the frame displacement \mathbf{v} . This form of the frame based formulation is suitable for comparison with the classical approach.

We write the linearisation of the first variation of the potential energy of the body on the non-barred side at the reference configuration in the form

$$\delta\pi_{\text{free}}^{\text{total}} = \delta\mathbf{u} \cdot (-\mathbf{f} + \mathbf{K}\mathbf{u}) \quad \text{with: } \mathbf{K} = \frac{\partial\mathbf{f}}{\partial\mathbf{u}} \quad (30)$$

and note that \mathbf{f} is the global load vector, matrix \mathbf{K} represents the stiffness matrix and vector \mathbf{u} stores the displacements at nodal points for the body on the non-barred side. A similar expression describes the behaviour of the body on the barred side.

The frame is discretised using 4-noded quads as described in the previous section. The bodies interact with the contact frame through a set of collocated forces applied at nodal points of the bodies. This is also described in more detail in the previous section. These discretisations are substituted into variational form (14). After carrying out the integrations and the linearisation about the reference configuration, we can add the governing equations of the discrete frame based contact formulation to the behaviour of the contacting bodies (given by equation (30) for the non-barred side) and obtain (see also ^[11])

$$\begin{bmatrix} \tilde{\mathbf{K}} & \tilde{\mathbf{B}} & \mathbf{0} \\ \tilde{\mathbf{B}}^t & \mathbf{0} & -\tilde{\mathbf{L}}_b \\ \mathbf{0} & -\tilde{\mathbf{L}}_b^t & \mathbf{0} \end{bmatrix} \begin{bmatrix} \tilde{\mathbf{u}} \\ \tilde{\boldsymbol{\lambda}} \\ \mathbf{v} \end{bmatrix} = \begin{bmatrix} \tilde{\mathbf{f}} \\ -\tilde{\mathbf{g}} \\ \mathbf{0} \end{bmatrix} \quad (31)$$

where

$$\begin{aligned} \tilde{\mathbf{K}} &= \begin{bmatrix} \mathbf{K} & \mathbf{0} \\ \mathbf{0} & \bar{\mathbf{K}} \end{bmatrix} ; & \tilde{\mathbf{B}} &= \begin{bmatrix} \mathbf{B} & \mathbf{0} \\ \mathbf{0} & \bar{\mathbf{B}} \end{bmatrix} ; & \tilde{\mathbf{L}}_b &= \begin{bmatrix} \mathbf{L}_b \\ \bar{\mathbf{L}}_b \end{bmatrix} \\ \tilde{\mathbf{u}} &= \begin{bmatrix} \mathbf{u} \\ \bar{\mathbf{u}} \end{bmatrix} ; & \tilde{\boldsymbol{\lambda}} &= \begin{bmatrix} \boldsymbol{\lambda} \\ \bar{\boldsymbol{\lambda}} \end{bmatrix} ; & \tilde{\mathbf{f}} &= \begin{bmatrix} \mathbf{f} \\ \bar{\mathbf{f}} \end{bmatrix} ; & \tilde{\mathbf{g}} &= \begin{bmatrix} \mathbf{g} \\ \bar{\mathbf{g}} \end{bmatrix} \end{aligned}$$

The vectors $\boldsymbol{\lambda}$ and $\bar{\boldsymbol{\lambda}}$ store the collocated contact forces on the non-barred and barred sides, respectively. Vector \mathbf{v} stores the displacements at nodal points of the contact frame. Equation (31)₁ is the equilibrium equation of the two contacting bodies. Equation (31)₂ is the gap constraint equation and equation (31)₃ is the frame equilibrium equation. It is noted that we have dropped the slip displacement variables from equation (31) for simplicity. Comparison with the classical formulation in the context of patch test passing abilities does not require to include slip variables.

We now rewrite equation (31) in the classical form (6) and start by expressing the solution of equation (31)₃ in the form

$$\tilde{\boldsymbol{\lambda}} = \mathbf{P}\boldsymbol{\lambda}^* \quad \text{with: } \mathbf{P} = \mathbf{I} - \tilde{\mathbf{L}}_b(\tilde{\mathbf{L}}_b^t\tilde{\mathbf{L}}_b)^{-1}\tilde{\mathbf{L}}_b^t \quad (32)$$

Premultiplying equation (31)₂ by $\tilde{\mathbf{L}}_b^t$ we find the frame displacements \mathbf{v} to be

$$\mathbf{v} = (\tilde{\mathbf{L}}_b^t\tilde{\mathbf{L}}_b)^{-1}\tilde{\mathbf{L}}_b^t(\tilde{\mathbf{g}} + \tilde{\mathbf{B}}^t\tilde{\mathbf{u}}) \quad (33)$$

The inverse of the matrix $\tilde{\mathbf{L}}_b^t\tilde{\mathbf{L}}_b$ needs to exist for this solution to be valid. This means that $\tilde{\mathbf{L}}_b$ must have full column-rank which is achieved by the frame design procedure outlined in the previous section. The remaining system of equations to be solved is given by

$$\begin{bmatrix} \tilde{\mathbf{K}} & \tilde{\mathbf{B}}\mathbf{P} \\ (\tilde{\mathbf{B}}\mathbf{P})^t & \mathbf{0} \end{bmatrix} \begin{bmatrix} \tilde{\mathbf{u}} \\ \boldsymbol{\lambda}^* \end{bmatrix} = \begin{bmatrix} \tilde{\mathbf{f}} \\ -\mathbf{P}\tilde{\mathbf{g}} \end{bmatrix} \quad (34)$$

This system of equations is singular since $\tilde{\mathbf{B}}\mathbf{P}$ does not have full column rank. To deal with this difficulty and without loss of generality, we represent $\boldsymbol{\lambda}^*$ by

$$\boldsymbol{\lambda}^* = [\boldsymbol{\Phi} \ \tilde{\mathbf{L}}_b] \begin{bmatrix} \hat{\boldsymbol{\lambda}} \\ \hat{\boldsymbol{\lambda}} \end{bmatrix} \quad \text{where: } \mathbf{P}\boldsymbol{\Phi} \neq \emptyset \text{ and } \mathbf{P}\tilde{\mathbf{L}}_b = \mathbf{0} \quad (35)$$

The $\boldsymbol{\lambda}^*$ space is spanned by the independent column vectors of $[\boldsymbol{\Phi} \ \tilde{\mathbf{L}}_b]$. Using this decomposition we can write equation (34) in the final form

$$\begin{bmatrix} \tilde{\mathbf{K}} & \tilde{\mathbf{B}}\mathbf{P}\boldsymbol{\Phi} \\ (\tilde{\mathbf{B}}\mathbf{P}\boldsymbol{\Phi})^t & \mathbf{0} \end{bmatrix} \begin{bmatrix} \tilde{\mathbf{u}} \\ \hat{\boldsymbol{\lambda}} \end{bmatrix} = \begin{bmatrix} \tilde{\mathbf{f}} \\ -\boldsymbol{\Phi}^t\mathbf{P}\tilde{\mathbf{g}} \end{bmatrix} \quad (36)$$

Comparing this equation to the classical form (6) shows that choosing $\mathbf{Q}^t = \tilde{\mathbf{B}}\mathbf{P}\Phi$ makes the classical formulation equivalent to the frame based formulation. The classical formulation will then be able to pass the contact patch test by following the frame design procedure outlined in the previous section. However, the resulting contact enforcement operator \mathbf{Q} will be dense (fully populated). This corresponds to some global interpolation of the Lagrange multipliers $\hat{\boldsymbol{\lambda}}$. It is well known that the master-slave approach described in section 3 fails the contact patch test. This is confirmed by our finding that the operator \mathbf{Q} needed to pass this test is dense, while the master-slave approach produces a sparse operator \mathbf{Q} .

7 3D patch test results

The optimised frame design is now used in the analysis of the proposed 3D contact patch test problem. Eight noded brick elements have been used for the discretisation of both the punch and foundation. We would like to recall that both the punch and the foundation have the same Poisson ratio. Therefore, we have based the design of the frame on the undeformed configuration. The frame will deform in lateral direction in the same way as the contacting bodies. As a result, the optimal relative position of the frame nodes with respect to the punch and foundation nodes is the same before and after deformation. The final deformation can be obtained in one step. We have used a *stick* state in the entire contact domain in this single computational step.

Several tables illustrate the computational results. Table 3 shows the position of the frame nodes after deformation. The “theoretical” results are obtained by multiplying the initial frame nodal x and y positions by 1.03. Obviously the downward displacement of the frame should be exactly 0.1 which should leave the frame at z=0.9. The “FEM result” columns show the frame positions resulting from the finite element analysis. These FEM results are in perfect agreement with the theoretical values.

Table 4 shows the normal forces acting on the frame from the punch and the foundation. The “theoretical” values are the ones obtained from the computation of energy equivalent forces corresponding to the constant normal pressure field between the punch and foundation. These forces have been used in the frame design process. Once again the FEM results are in perfect agreement with the theoretical values.

Table 5 shows some maximum deviations from exact values for selected quantities. These deviations are of the order of magnitude of the roundoff errors in the computational model. Therefore, we can conclude that our frame based contact

frame node	x-coordinate		y-coordinate		z-coordinate	
	theoretical	FEM result	theoretical	FEM result	theoretical	FEM result
1	0.217806	0.217806	0	0.000000	0.9	0.900000
2	0.580936	0.580936	0	0.000000	0.9	0.900000
3	1.0815	1.081500	0	0.000000	0.9	0.900000
4	0.349844	0.349844	0.381872	0.381872	0.9	0.900000
5	0.707499	0.707499	0.309175	0.309175	0.9	0.900000
6	1.0815	1.081500	0.061811	0.061811	0.9	0.900000
7	0.186905	0.186905	0.997985	0.997985	0.9	0.900000
8	0.625347	0.625347	0.752681	0.752681	0.9	0.900000
9	1.0815	1.081500	0.632736	0.632736	0.9	0.900000
10	0.219517	0.219517	1.0815	1.081500	0.9	0.900000
11	0.432560	0.432560	1.0815	1.081500	0.9	0.900000
12	1.0815	1.081500	1.0815	1.081500	0.9	0.900000

Table 3: Position of the frame nodal points after deformation (see Figure 11 for the frame node numbering).

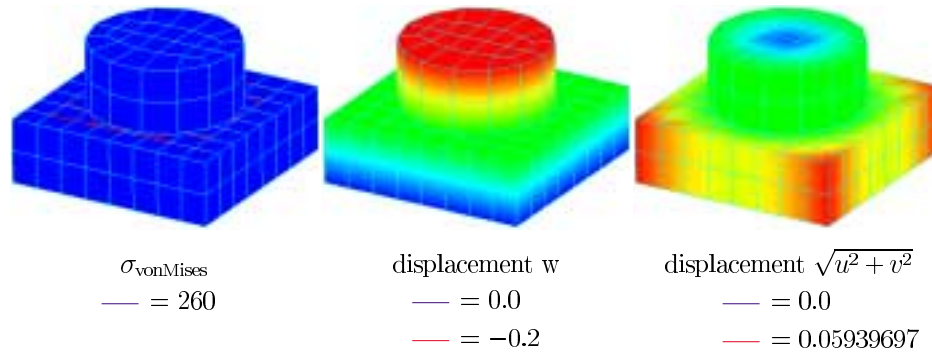


Figure 13: Computed von Mises stress and displacements.

model performs excellently in the 3D contact patch test problem.

Finally, Figure 13 shows the von Mises stress in the entire model. The exact value of 260 for this stress is obtained in the FEM analysis as indicated by the solid blue colour. The remaining two deformation plots show the displacement distribution in the model.

node	nodal normal force acting on foundation		nodal normal force acting on punch	
	theoretical	FEM result	theoretical	FEM result
1	31.850000	31.850000	31.241534	31.241534
2	31.850000	31.850000	24.778470	24.778470
3	31.040561	31.040562	21.101634	21.101634
4	9.761253	9.761253	13.548987	13.548987
5	31.850000	31.850000	41.236884	41.236884
6	31.849998	31.849998	30.992300	30.992300
7	28.694115	28.694115	16.144860	16.144860
8	5.933156	5.933156	13.959140	13.959140
9	31.053523	31.053523	21.492565	21.492565
10	28.686091	28.686091	28.256039	28.256039
11	14.321187	14.321187	—	—
12	0.689455	0.689455	—	—
13	9.642879	9.642878	—	—
14	5.971022	5.971022	—	—
15	0.710470	0.710470	—	—

Table 4: Normal forces between the frame, the foundation and the punch (see Figure 11 for the punch and foundation node numbering; compression defined positive).

	absolute	relative
max. z-pos. error of frame nodes	$2.50 * 10^{-10}$	$2.78 * 10^{-10}$
max. σ_{vonMises} error in punch	$1.00 * 10^{-6}$	$3.85 * 10^{-9}$
max. σ_{vonMises} error in foundation	$1.00 * 10^{-6}$	$3.85 * 10^{-9}$
max. frictional force	$1.15 * 10^{-7}$	—

Table 5: Deviations from exact values due to roundoff effects.

8 Conclusion

In this paper we have presented our frame based contact model in the context of 3D contact modelling. The crucial element in our formulation is the design of the contact frame between nonmatching meshes. The design of the contact frame has been based a priori on the requirement that the formulation must be able to produce theoretically exact results in patch test conditions. We have proposed a 3D contact patch test. It is nontrivial and has similar features as its 2D counterpart. We have used it to validate our frame based formulation with excellent results.

Acknowledgements

The present work has been supported by Sandia National Laboratories under the Accelerated Strategic Computational Initiative (ASCI) contract AS-5666 and by Lawrence Livermore National Laboratories under the Scalable Algorithms for Massively Parallel Computations (ASCI level-II) contract B347880.

References

1. Bathe, K. J., Chaudhary, A. ‘A solution method for planar and axisymmetric contact problems’. *International Journal for Numerical Methods in Engineering*, Vol. 21, pp. 65–88, 1985.
2. Casey, J. ‘On finitely deforming rigid-plastic materials’. *International Journal of Plasticity*, Vol. 2, pp. 247–277, 1986.
3. Francavilla, A., Zienkiewicz, O. C. ‘A note on numerical computation of elastic contact problems’. *International Journal for Numerical Methods in Engineering*, Vol. 9, pp. 913–924, 1975.
4. Hallquist, J. O. ‘Nike2D—a vectorized, implicit, finite deformation, finite element code for analyzing the static and dynamic response of 2-d solids’. *RPT. UCRL-52678*, LLNL, Livermore, 1979.
5. Hallquist, J. O., Goudreau, G. L., Benson, D. J. ‘Sliding interfaces with contact-impact in large-scale Lagrangian computations’. *Computer Methods in Applied Mechanics and Engineering*, Vol. 51, pp. 107–137, 1985.
6. Hughes, T. J. R., Taylor, R. L., Sackman, J. L., Curnier, A., Kanoknukulchai, W. ‘A finite element method for a class of contact-impact problems’. *Computer Methods in Applied Mechanics and Engineering*, Vol. 8, pp. 249–276, 1976.

7. Jones, R. E., Papadopoulos P. ‘A yield-limited Lagrange multiplier formulation for frictional contact’. *International Journal for Numerical Methods in Engineering*, Vol. 48, pp. 1127–1149, 2000.
8. MacNeal, R. H. ‘Finite Elements: Their Design and Performance’. in: *Mechanical Engineering*, Vol. 89, Marcel Dekker, Inc., New York/Basel/Hong Kong, 1994.
9. Papadopoulos, P., Taylor, R. L. ‘A Mixed Formulation for the Finite Element Solution of Contact Problems’. *Computer Methods in Applied Mechanics and Engineering*, Vol. 94, pp. 373–389, 1992.
10. Rebel, G., Park, K. C., Felippa, C. A. ‘A Contact-Impact Formulation Based on Localized Lagrange Multipliers’. Report CU-CAS-00-18, College of Engineering, University of Colorado at Boulder, July 2000.
11. Rebel, G., Park, K. C., Felippa, C. A. ‘A Contact Formulation Based on Localized Lagrange Multipliers: Formulation and Application to Two-dimensional Problems’. ... *to be published in IJNME*
12. Simo, J. C., Wriggers, P., Schweizerhof, K. H., Taylor, R. L. ‘Finite deformation postbuckling analysis involving inelasticity and contact constraints’. University of California at Berkeley, *Report No. UCB/SESM-84/15*, Berkeley, 1984.
13. Taylor, R. L., Papadopoulos, P. ‘On a Patch Test for Contact Problems in Two Dimensions’. in: *Wriggers, P., Wagner, W., eds., Nonlinear Computational Mechanics*, pp 690–702, Springer, Berlin, 1991.
14. Zhong, Z. H. ‘On Numerical Procedures for Contact Problems’. Licentiate Thesis, 1987:02L, Luleå University, Luleå, 1987.
15. Zhong, Z. H. ‘On contact-impact problems’. Dissertation No. 178, Linköping University, Linköping, 1988.
16. Zhong, Z. H. ‘Finite Element Procedures for Contact-Impact Problems’. Oxford University Press, Oxford, 1993.